Published in Optics Express, 21, issue 5, 5781-5792, 2013
which should be used for any reference to this work

Metrological characterization of custom-designed 894.6 nm VCSELs for miniature atomic clocks

F. Gruet,[1] A. Al-Samaneh,[2] E. Kroemer,[3] L. Bimboes,[1,4] D. Miletic,[1] C. Affolderbach,[1,*] D. Wahl,[2] R. Boudot,[3,5] G. Mileti,[1] and R. Michalzik[2,6]

[1] *Time and Frequency Laboratory (LTF), Physics Department, University of Neuchâtel, Avenue de Bellevaux 51, 2000 Neuchâtel, Switzerland*
[2] *Institute of Optoelectronics, Ulm University, 89069 Ulm, Germany*
[3] *FEMTO-ST, CNRS, 32 Avenue de l'Observatoire 25044 Besançon cedex, France*
[4] *on leave from Institut d'Optique Graduate School, 91127 Palaiseau cedex, France*
[5] *rodolphe.boudot@femto-st.fr*
[6] *rainer.michalzik@uni-ulm.de*
[*] *christoph.affolderbach@unine.ch*

Abstract: We report on the characterization and validation of custom-designed 894.6 nm vertical-cavity surface-emitting lasers (VCSELs), for use in miniature Cs atomic clocks based on coherent population trapping (CPT). The laser relative intensity noise (RIN) is measured to be 1×10^{-11} Hz^{-1} at 10 Hz Fourier frequency, for a laser power of 700 μW. The VCSEL frequency noise is $10^{13} \cdot f^{-1}$ Hz^2/Hz in the 10 Hz $< f <$ 10^5 Hz range, which is in good agreement with the VCSEL's measured fractional frequency instability (Allan deviation) of $\approx 1 \times 10^{-8}$ at 1 s, and also is consistent with the VCSEL's typical optical linewidth of 20–25 MHz. The VCSEL bias current can be directly modulated at 4.596 GHz with a microwave power of -6 to $+6$ dBm to generate optical sidebands for CPT excitation. With such a VCSEL, a 1.04 kHz linewidth CPT clock resonance signal is detected in a microfabricated Cs cell filled with Ne buffer gas. These results are compatible with state-of-the-art CPT-based miniature atomic clocks exhibiting a short-term frequency instability of 2–3$\times 10^{-11}$ at $\tau = 1$ s and few 10^{-12} at $\tau = 10^4$ s integration time.

OCIS codes: (020.1670) Coherent optical effects; (120.3930) Metrological instrumentation; (250.7269) Vertical cavity surface emitting lasers; (300.6320) Spectroscopy, high-resolution.

References and links

1. E. Arimondo, "Coherent population trapping in laser spectroscopy," Prog. Opt. **35**, 257–354 (1996).
2. S. Knappe, "MEMS atomic clocks," in *Comprehensive Microsystems*, Y. Gianchandani, O. Tabata, and H. Zappe eds. (Elsevier B.V., 2010), **3**, pp. 571–612.
3. C. Affolderbach, A. Nagel, S. Knappe, C. Jung, D. Wiedenmann, and R. Wynands, "Nonlinear spectroscopy with a vertical-cavity surface-emitting laser," Appl. Phys. B **70**, 407–413 (2000).
4. M. Stähler, R. Wynands, S. Knappe, J. Kitching, L. Hollberg, A. Taichenachev, and V. Yudin, "Coherent population trapping resonances in thermal ^{85}Rb vapor: D_1 versus D_2 line excitation," Opt. Lett. **27**, 1472–1474 (2002).
5. R. Lutwak, D. Emmons, T. English, W. Riley, A. Duwel, M. Varghese, D. K. Serkland, and G. M. Peake, "The chip-scale atomic clock – recent development progress," in *Proceedings of the 35$^{\text{th}}$ Precise Time and Time Interval Systems Applications Meeting (PTTI 2003)*, L. Breakiron ed. (US Naval Observatory, 2003), 467–478.

6. D. K. Serkland, G. M. Peake, K. M. Geib, R. Lutwak, R. M. Garvey, M. Varghese, and M. Mescher, "VCSELs for atomic clocks," Proc. SPIE **6132**, 613208 (2006).
7. A. Al-Samaneh, M. Bou Sanayeh, S. Renz, D. Wahl, and R. Michalzik, "Polarization control and dynamic properties of VCSELs for MEMS atomic clock applications," IEEE Photon. Technol. Lett. **23**, 1049–1051 (2011).
8. R. Michalzik, "VCSEL fundamentals," Chap. 2 in *VCSELs*, R. Michalzik ed., Springer Series in Optical Sciences **166** (Springer, 2013), pp. 19–75.
9. A. Al-Samaneh, S. Renz, A. Strodl, W. Schwarz, D. Wahl, and R. Michalzik, "Polarization-stable single-mode VCSELs for Cs-based MEMS atomic clock applications," in *Semiconductor Lasers and Laser Dynamics IV*, Proc. SPIE **7720**, 772006 (2010).
10. A. Al-Samaneh, M. Bou Sanayeh, M. J. Miah, W. Schwarz, D. Wahl, A. Kern, and R. Michalzik, "Polarization-stable vertical-cavity surface-emitting lasers with inverted grating relief for use in microscale atomic clocks," Appl. Phys. Lett. **101**, 171104 (2012).
11. J. M. Ostermann and R. Michalzik, "Polarization control of VCSELs," Chap. 5 in *VCSELs*, R. Michalzik ed., Springer Series in Optical Sciences **166** (Springer, 2013), pp. 147–179.
12. G. Di Domenico, S. Schilt, and P. Thomann, "Simple approach to the relation between laser frequency noise and laser line shape," Appl. Opt. **49**, 4801–4807 (2010).
13. R. Wynands and A. Nagel, "Inversion of frequency-modulation spectroscopy line shapes," J. Opt. Soc. Am. B **16**, 1617–1622 (1999).
14. R. Lutwak, A. Rashed, M. Varghese, G. Tepolt, J. Leblanc, M. Mescher, D. K. Serkland, K. M. Geib, and G. M. Peake, "CSAC: The chip scale atomic clock," in *Proceedings of the 7th Symp. Freq. Standards and Metrology*, L. Maleki ed. (World Scientific, 2008), 454–462.
15. J. C. Camparo and J. G. Coffer, "Conversion of laser phase noise to amplitude noise in a resonant atomic vapor: The role of laser linewidth," Phys. Rev. A **59**, 728–735 (2005).
16. D. Miletic, C. Affolderbach, M. Hasegawa, R. Boudot, C. Gorecki, and G. Mileti, "AC Stark-shift in CPT-based Cs miniature atomic clocks," Appl. Phys. B **109**, 89–97 (2012).
17. E. Rubiola, *Phase Noise and Frequency Stability of Oscillators* (Cambridge University, 2010), Chap. 1.
18. X. Liu and R. Boudot, "A distributed-feedback diode laser frequency stabilized on Doppler-free Cs D_1 line," IEEE Trans. Instr. Meas. **61**, 2852–2855 (2012).
19. S. Knappe, R. Wynands, J. Kitching, H. G. Robinson, and L.Hollberg "Characterization of coherent population-trapping resonances as atomic frequency references," J. Opt. Soc. Am. B **18**, 1545–1553 (2001).
20. M. Hasegawa, R. K. Chutani, C. Gorecki, R. Boudot, P. Dziuban, V. Giordano, S. Clatot, and L. Mauri, "Microfabrication of cesium vapor cells with buffer gas for MEMS atomic clocks," Sensors Actuat. A: Phys. **167**, 594–601 (2011).
21. D. Miletic, P. Dziuban, R. Boudot, M. Hasegawa, R. K. Chutani, G. Mileti, V. Giordano, and C. Gorecki, "Quadratic dependence on temperature of Cs 0-0 hyperfine resonance frequency in single Ne buffer gas microfabricated vapor cell," Electron. Lett. **46**, 1069–1071 (2010).
22. R. Boudot, P. Dziuban, M. Hasegawa, R. K. Chutani, S. Galliou, V. Giordano, and C. Gorecki, "Coherent population trapping resonances in Cs-Ne vapor microcells for miniature clocks applications," J. Appl. Phys. **109**, 014912 (2011).
23. O. Kozlova, S. Guérandel, and E. De Clercq, "Temperature and pressure shifts of the Cs clock transition in the presence of buffer gases: Ne, N_2, Ar," Phys. Rev. A **83**, 062714 (2011).
24. F. Gruet, L. Bimboes, D. Miletic, C. Affolderbach, G. Mileti, A. Al-Samaneh, D. Wahl, and R. Michalzik, "Spectral characterisation of VCSELs emitting at 894 nm for CPT-based miniature atomic clocks," in *Proceedings of the Conference on Lasers and Electro-Optics Europe, CLEO/Europe 2011*, Munich, Germany, May 2011, paper CB.P.27.
25. M. Huang and J. Camparo, "The influence of laser polarization variations on CPT atomic clock signals," in *Proceedings of the Joint Conference of the IEEE International Frequency Control Symposium & European Frequency and Time Forum* (The Institute of Electrical and Electronics Engineers Inc., 2011), 951–954.

1. Introduction

Over recent years, CPT physics [1] combined with micro-electromechanical systems (MEMS) fabrication techniques and semiconductor lasers has allowed the development of miniature atomic clocks exhibiting a low power consumption ($\approx$ 150 mW), a volume of 10–15 cm^3 and frequency stability performances better than 10^{-11} at 1 hour to 1 day of integration time [2]. These miniature atomic frequency standards outperform widely-used traditional quartz-crystal oscillators and are promising for a number of civil, industrial and military applications such as mobile telecommunications, telecommunication and power networks, navigation systems or sensor applications. Current miniature CPT clocks use a VCSEL to generate optical sidebands

for CPT excitation. These compact, low-power, low-threshold current and high-modulation-bandwidth lasers—despite their broad linewidth (100 MHz typically)—have demonstrated their potential to detect narrow-linewidth CPT resonances in alkali vapor cells [3]. Later, it was shown that excitation on the D_1 line results in higher contrast and narrower CPT resonances than excitation on the D_2 line, for Rb [4] as well as for Cs [5]. While VCSELs on the Rb D_1 line can be found easily, VCSELs emitting on the Cs D_1 line at 894.6 nm are not commercially available yet. Sandia National Laboratories are known to develop high-performance 894.6 nm VCSELs for DARPA CSACs projects [6] but, to our knowledge, these components remain unaccessible for other customers. Recently, Al-Samaneh *et al.* reported on the technology description, polarization stability and small-signal characteristics of novel custom-designed polarization-stable and single-mode VCSELs emitting at 894.6 nm wavelength [7]. In the present communication we demonstrate high-level performance of very similar VCSELs (described in section 2) and prove their suitability for chip-scale atomic clocks. Section 3 reports several metrological characterizations of the VCSELs, including modulation capabilities, emission linewidth, relative intensity noise (RIN), frequency noise, and frequency stability (Allan deviation) measurements. In section 4, a 894.6 nm VCSEL is used as a laser source in a compact CPT clock demonstrator based on a microfabricated Cs cell.

2. 894.6 nm VCSEL description

The VCSELs are grown on n-doped (100)-oriented GaAs substrates using solid-source molecular beam epitaxy. The active region consists of three compressively strained 8 nm thick InGaAs quantum wells (QWs) with 6 % or 4 % indium content. The QWs are placed in an antinode of the standing-wave pattern to achieve a good coupling between electrons and photons. The inner cavity is one material wavelength thick with the active region sandwiched between two larger bandgap $Al_{0.47}Ga_{0.53}As$ cladding layers. A highly p-doped 30 nm thick AlAs layer is grown directly above the top cladding layer at a node of the standing-wave pattern. Current confinement and weak optical index guiding are achieved by wet-chemical oxidation of the AlAs layer. The n-type bottom and p-type top distributed Bragg reflectors (DBRs) consist of 38.5 Si-doped and 25 C-doped $Al_{0.90}Ga_{0.10}As/Al_{0.20}Ga_{0.80}As$ layer pairs, respectively. The DBRs are graded in composition and doping concentration to minimize the free-carrier absorption and decrease the electrical resistance [8]. In this work two different VCSEL designs have been utilized. Both have a top annular p-contact but either a substrate-side or a top n-contact which serve for current injection. We refer to the first design as *a standard VCSEL*. Figure 1 shows such a VCSEL chip having $250 \times 250\ \mu m^2$ size.

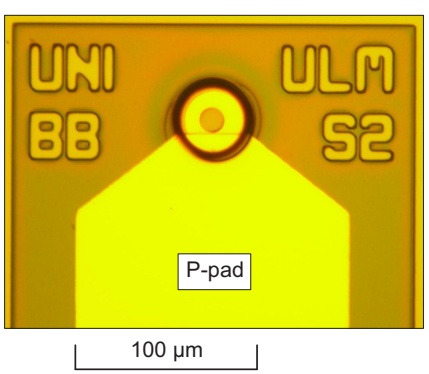

Fig. 1. Photograph of a fully processed VCSEL with a standard n-type substrate-side contact, suitable for wire bonding of the p-contact.

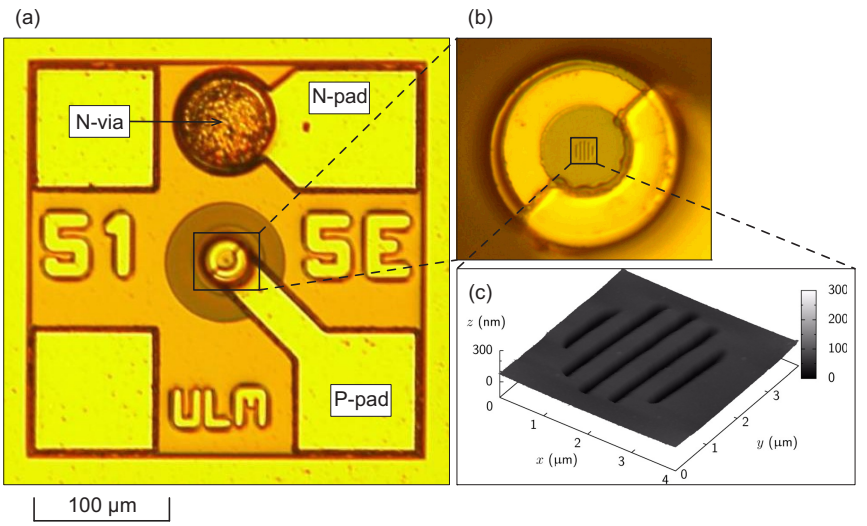

Fig. 2. (a) Photograph of a fully processed flip-chip-bondable VCSEL with an inverted grating relief. (b) Zoomed outcoupling facet. (c) Surface profile within the grating relief region measured with an AFM. The grating relief has a diameter of 3 μm, a grating period of 0.6 μm, and an etch depth of 70 nm.

The latter VCSEL has a *flip-chip-bondable* design [9]. By etching a mesa down to the first layer pairs of the n-type DBR and applying a polyimide passivation layer that contains a circular hole for a Au-electroplated n-via, the n-contact becomes accessible from the epitaxial side of the chip. This is seen in Fig. 2 (a), which shows the VCSEL chip with 300×300 μm^2 size. In addition, this chip design applies the so-called inverted grating relief [10] by which favorable single-mode and polarization-stable laser emission is achieved. The surface grating is etched in an extra topmost GaAs quarter-wave antiphase layer. Figs. 2(b) and (c) show the grating relief and its surface profile measured with an atomic force microscope (AFM). Grating reliefs with 3 μm diameter, quarter-wave etch depth, sub-emission-wavelength grating periods of 0.6 μm, and 50 % duty cycle have been employed. The grating grooves are etched along the [011] GaAs crystal axis. Figure 3 depicts a cross-sectional view of the flip-chip-bondable VCSEL from Fig. 2.

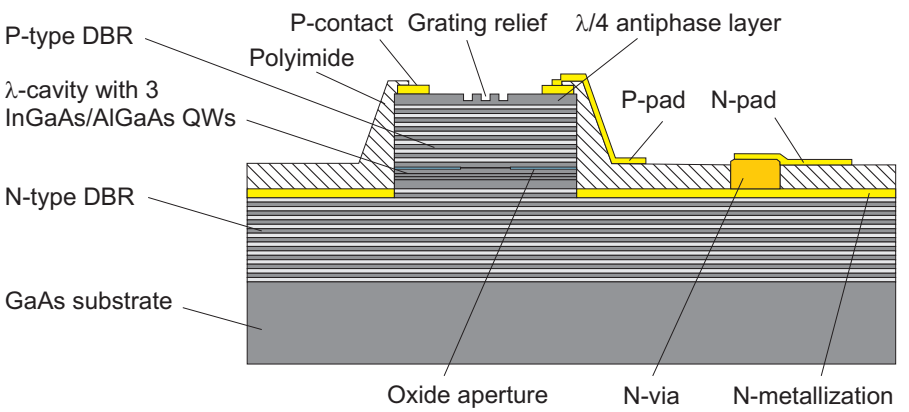

Fig. 3. Schematic cross-section of the flip-chip bondable VCSEL with inverted grating relief. λ denotes the material wavelength.

2.1. *Standard VCSELs*

Several standard VCSELs have been mounted in TO-46 cans for convenient testing. Having substrate-side n-contacts, the laser chips were fixed on silicon submounts by conductive glue. The anode of the TO-46 can is wire-bonded to the top p-pad while the cathode is wire-bonded to the Au-metalized top of the silicon submount. An external lens is employed for laser beam collimation. A thermoelectric cooler (TEC) and a thermistor are fixed in proximity of the VCSEL package for temperature control. The polarization of the light emitted from standard VCSELs is a priori undefined. Often, a majority of standard VCSELs on a wafer has equal polarization. However, the polarization can easily switch to an orthogonal direction upon changes of the bias current or the operating temperature [11]. Devices with stable polarization in the operation range of interest have been selected. The polarization-resolved light–current–voltage (PR-LIV) characteristics of such a laser are shown in Fig. 4.

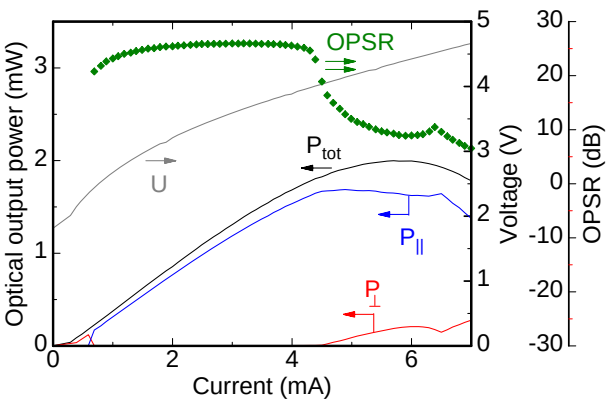

Fig. 4. Polarization-resolved operation characteristics of a standard VCSEL with 3 μm active diameter at 23°C substrate temperature. P_{tot}: total optical power; $P_{\parallel}$, $P_{\perp}$: optical powers for light polarized parallel and orthogonal to the reference axis, respectively; U: applied voltage.

Single-mode emission polarized parallel to the [011] GaAs crystal axis is maintained up to a current of 4.4 mA. Over this range, the orthogonal polarization suppression ratio (OPSR) is greater than 20 dB, where $\mathrm{OPSR} = 10\log(P_{\parallel}/P_{\perp})$. $P_{\parallel}$ and $P_{\perp}$ are the optical powers measured behind a Glan–Thompson polarizer whose transmission direction is oriented parallel and orthogonal to the reference axis, respectively. Losses of the polarizer are responsible for $P_{\parallel} + P_{\perp} < P_{\mathrm{tot}}$ in Fig. 4.

Figure 5 depicts the optical spectrum at 23°C. The Cs D_1 line wavelength of 894.6 nm is reached at a current of 2.1 mA. The side-mode suppression ratio (SMSR) is about 42 dB. This laser was utilized to resolve all four hyperfine components of the Cs D_1 line, which are clearly separated in Fig. 6. The corresponding atomic transitions link the Cs ground-state levels ($6^2S_{1/2}$, total atomic angular momentum $F = 3$ or 4) to the lowest excited-state levels ($6^2P_{1/2}$, total atomic angular momentum $F' = 3$ or 4), and the observed relative line strengths are in agreement with the relative weights expected from theory. The VCSEL was operated at a temperature of 23°C and a current of about 2.1 mA. Frequency detuning at a rate of ≈ 300 GHz/mA was achieved by sweeping the laser current, and of ≈ 0.06 nm/K by acting on the laser temperature.

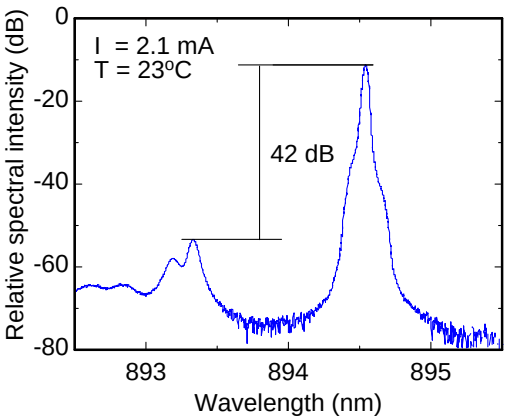

Fig. 5. Spectrum of the VCSEL from Fig. 4 at 2.1 mA current and 23°C substrate temperature.

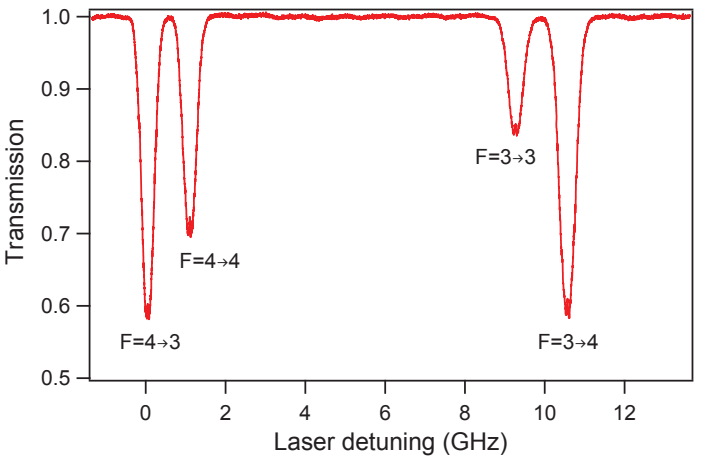

Fig. 6. Cs D_1 absorption lines observed when transmitting the light of the VCSEL from Fig. 4 through a Cs vapor cell.

2.2. Grating relief VCSELs

Several flip-chip bondable VCSELs according to the design in Fig. 2 have been mounted in TO-46 cans. Having top n-contacts, such VCSELs were fixed on silicon submounts using conductive glue. The anode and cathode of the TO-46 can were wire-bonded to the top p- and n-pads of the VCSEL. For temperature control, a TEC and a thermistor are placed inside the can. PR-LIV characteristics of a grating relief VCSEL at 30°C substrate temperature are shown in Fig. 7. Five times $P_{\|}$ is plotted here for better clarity.

The device remains polarization-stable up to thermal roll-over with a maximum magnitude of the OPSR of 22.7 dB. The polarization of inverted grating VCSELs with optimum design is always orthogonal to the grating lines [10], resulting in an opposite sign of the OPSR in Fig. 7 compared to Fig. 4. Figure 8 depicts polarization-resolved spectra at 30°C. The target wavelength is reached at a current of 1.4 mA with an SMSR of about 40 dB and a peak-to-peak difference between the dominant and the suppressed polarization modes of almost 29 dB.

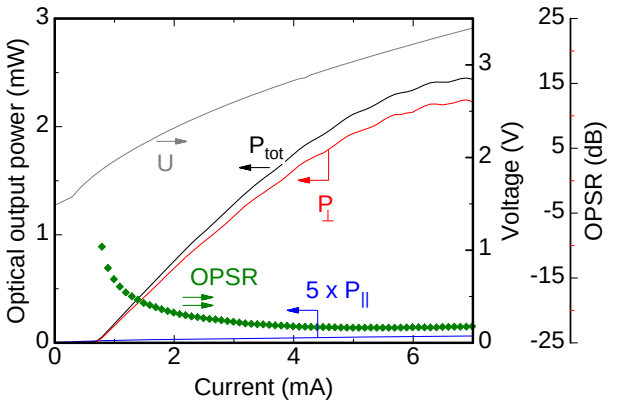

Fig. 7. Polarization-resolved operation characteristics of a grating relief VCSEL with 3.6 μm active diameter at 30°C substrate temperature. The grating relief has a diameter of 3 μm, a grating period of 0.6 μm and an etch depth of 70 nm.

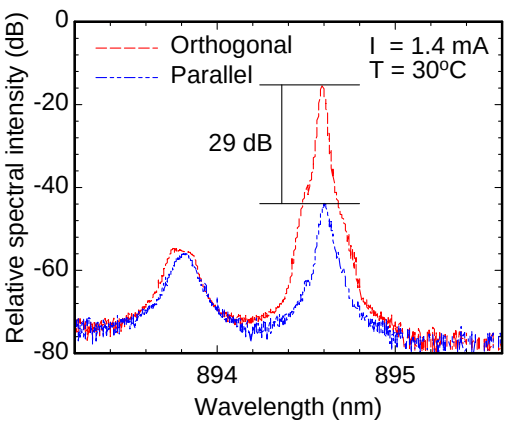

Fig. 8. Polarization-resolved spectra of a grating relief VCSEL at 1.4 mA bias current.

3. Laser noise and dynamics

Standard VCSELs show threshold currents of around 0.3 mA (see Fig. 4), depending only weakly on the VCSEL temperature (≤ 2 μA/K in the 15°C to 25°C range). The Cs D_1 line wavelength is reached at a direct current of 2.1 mA and a VCSEL temperature of 23°C, giving an output power of 910 μW and > 40 dB SMSR.

Figure 9 shows a spectrum of the VCSEL's optical linewidth, measured with a high-resolution Fabry–Pérot interferometer (5 MHz intrinsic linewidth). Typical linewidths measured are around 20–25 MHz, which also allows resolving saturated-absorption lines (see the inset in Fig. 9) [3]. An independent determination of the VCSEL linewidth can be obtained from the power spectral density (PSD) of the laser's frequency fluctuations $S_{\Delta\nu}(f)$ shown in Fig. 10. In our case, the VCSEL linewidth Γ can be estimated as $\Gamma = \sqrt{8A\ln 2}$, where A is the integral over $S_{\Delta\nu}(f)$ [12]. This method gives $\Gamma \approx 20$ MHz, in good agreement with the linewidths measured with the Fabry–Pérot interferometer.

The VCSEL's bias current was modulated at half of the Cs hyperfine frequency (i.e., at $\omega_m =$ 4.596 GHz), in order to create optical sidebands frequency-separated by 9.192 GHz as required

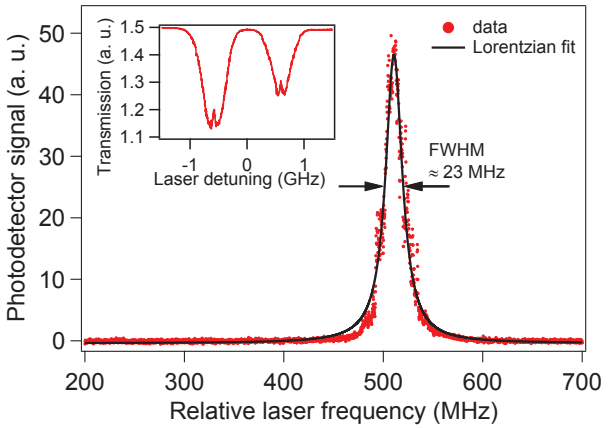

Fig. 9. Linewidth measurement of the VCSEL when operating at the Cs D_1 line. The Fabry–Pérot linewidth is 5 MHz and the total sweeptime for this graph is 30 ms. The inset shows narrow saturated-absorption features of the Cs D_1 line $F_g = 4$ component recorded in an evacuated Cs cell.

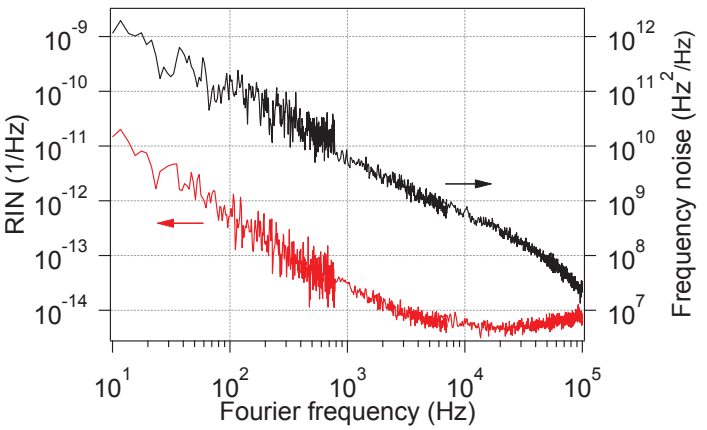

Fig. 10. Relative intensity noise (RIN; red bottom trace) and frequency noise (black upper trace) of the VCSEL diode in free-running regime, operating in resonance with the Cs D_1 line.

for CPT interaction [3]. Figure 11 presents the relative strength of the carrier and first-order sidebands, measured with a Fabry–Pérot interferometer.

The electric field $E(t)$ emitted by the modulated VCSEL is described by

$$E(t) = E_0[1 + R\sin(\omega_m t + \Psi)]\cos(\omega_0 t + M\sin(\omega_m t)) \quad (1)$$

where ω_0 is the optical laser carrier frequency, M and R are the phase and amplitude modulation indices, respectively, and Ψ the relative phase between both modulations effects [13]. Figure 11 also gives the values of M and R, extracted by fitting the sideband powers resulting from Eq. (1) [13] to the experimental data, which takes into account asymmetric sidebands (due to residual amplitude modulation) via the amplitude modulation index R. The sideband asymmetry S (defined as $S = -10\log(P_{+1}/P_{-1})$, where P_{+1} and P_{-1} are the power of the positive and negative first-order sidebands, respectively) remains essentially constant for all applied modu-

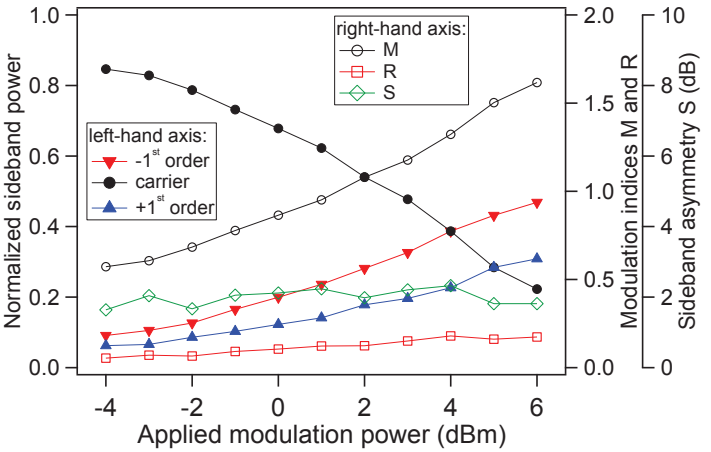

Fig. 11. Normalized sideband power (filled symbols, left-hand axis) and corresponding modulation indices M and R and sideband asymmetry S (open symbols, right-hand axis) for different power levels of the 4.596 GHz modulation frequency applied to the VCSEL.

lation powers. Both first-order sidebands become stronger than the carrier at modulation powers $\geq +5$ dBm. Limitations in modulation efficiency can be attributed to imperfect coupling of the radio-frequency signal into the lasers' TO-46 cans, which is evidenced by $\approx 40\%$ of the applied 4.6 GHz modulation power being reflected by the VCSEL and its TO-46 can.

Figure 10 reports the measured RIN and frequency noise of the VCSEL when emitting in resonance with the Cs D_1 line. The RIN is measured to be 1×10^{-11} Hz^{-1} at 10 Hz and 5×10^{-15} Hz^{-1} at 10 kHz Fourier frequencies. The frequency noise of the VCSEL is known to be one of the main limitations to the short-term frequency stability of miniature atomic clocks [14], due to frequency-to-amplitude noise conversion in the atomic vapor that degrades the clock's signal-to-noise ratio [5, 15]. As a second effect, the laser frequency noise also limits the frequency stability achievable for the frequency-stabilized laser, which at longer integration times can result in significant clock instability contributions via the frequency light-shift effect [16], as detailed in the following. The PSD of frequency fluctuations $S_{\Delta\nu}(f)$ of the free-running VCSEL diode (see Fig. 10) is measured as $S_{\Delta\nu}(10\text{ Hz}) = 10^{12}$ Hz^2/Hz with a f^{-1} slope that is signature of a flicker frequency noise. The PSD of *relative* frequency fluctuations is described in terms of $S_y(f) = S_{\Delta\nu}/\nu_0^2$ where ν_0 is the laser frequency (3.35×10^{14} Hz). Describing the frequency noise spectrum by the power law model $S_y(f) = \sum_{i=-2}^{2} h_i f^i$, we obtain $h_{-1} = 10^{13}/\nu_0^2 = 8.9 \times 10^{-17}$. This yields an expected laser frequency stability (in terms of Allan deviation) of $\sigma_y(\tau = 1s) = \sqrt{h_{-1} 2\ln 2} = 1.1 \times 10^{-8}$ [17]. In order to verify this estimation, we measured the relative frequency stability of the VCSEL in the free-running and frequency-stabilized regimes (see Fig. 12) by detecting the frequency beatnote between the VCSEL and a narrow-linewidth distributed feedback (DFB) laser [18].

The laser frequency is stabilized on the position of maximum optical absorption of a cm-scale reference Cs cell by modulating the laser direct current at 60 kHz and demodulating the absorption signal on a photodiode with a lock-in amplifier. The resulting correction signal was applied to the VCSEL current, thus providing sufficiently high servo bandwidth. No radio frequency modulation is applied. In the free-running regime, the short-term frequency stability is measured as 1×10^{-8} at 1 s, in agreement with the frequency noise measurements. For the frequency-stabilized VCSEL the stability is improved to 8×10^{-9} at 1 s and to about 4×10^{-9} at 10^4 s integration time. We use this latter result and a frequency-light-shift coefficient of

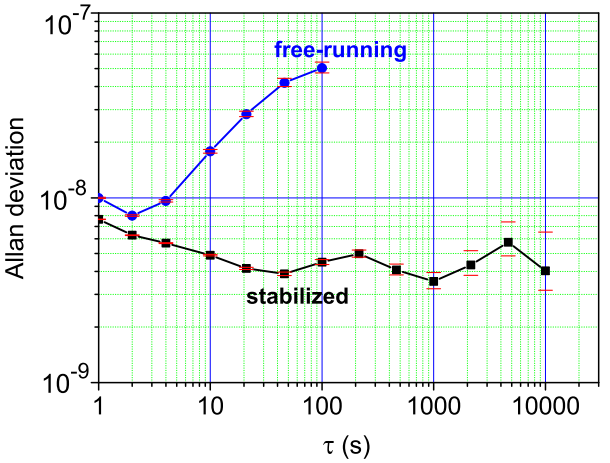

Fig. 12. Allan deviation of the VCSEL frequency, in frequency-stabilized and free-running regimes. The VCSEL is locked to the center of a homogeneously broadened optical Cs absorption line.

$\delta\nu_{clock}/\delta\nu_0 = -20$ mHz/MHz reported for VCSEL-driven CPT [19] to estimate the impact on the clock stability. The resulting clock instability contribution from the frequency light-shift is on the level of 2×10^{-12} at $\tau \approx 10^4$ s, which is compatible with the typical specifications for miniature atomic clocks.

4. CPT clock experiment

Figure 13 shows a simplified scheme of the Cs CPT clock experimental setup. The laser source is a custom-designed grating relief VCSEL resonant at 894.6 nm developed by Ulm University, as described in Section 2.2. It is operated at 1.3 mA and 30°C, to be resonant with the Cs D_1 line. The linewidth of the grating relief VCSEL is measured to be ≈ 25 MHz, comparable to those reported in section 3 for the standard VCSELs. The optical output of the laser is collimated into a 2-mm diameter beam and sent through a linear polarizer and a quarter-wave plate. The laser power incident to the Cs cell is about 22 μW. The injection current of the laser is directly modulated at 4.596 GHz using a commercial frequency synthesizer and the modulation power was adjusted to -2 dBm for maximum CPT signal height. The Cs microfabricated cell, realized according to the process described in [20], is 2 mm in diameter, 1.4-mm long, and is filled with Ne buffer gas. The cell is temperature-stabilized to ≈ 80°C where the temperature-dependence of the Cs clock frequency is cancelled [21–23]. A static magnetic field of several μT is applied to the cell, placed in a single-layer mu-metal magnetic shield. The laser power is detected at the output of the cell with a photodiode that provides signals for two servo loops. The first one serves to stabilize the laser frequency to the center of the homogeneously-broadened optical absorption line; the second one provides the CPT signal and can be used to stabilize the local oscillator (LO) frequency to the center of the CPT resonance for clock operation.

Figure 14 displays the CPT clock resonance signal fitted by a Lorentzian profile. The CPT linewidth is 1.04 kHz at 80°C cell temperature and does not vary significantly in the 70–90°C range (CPT signals with only slightly larger linewidth were observed previously [24] using the standard VCSELs described in section 2.1). The contrast C (ratio between the signal amplitude S and the background B) is 0.93 %. The corresponding error signal has a discriminator slope D of typically 0.9×10^{-6} V/Hz. The detection noise N at the LO modulation frequency is

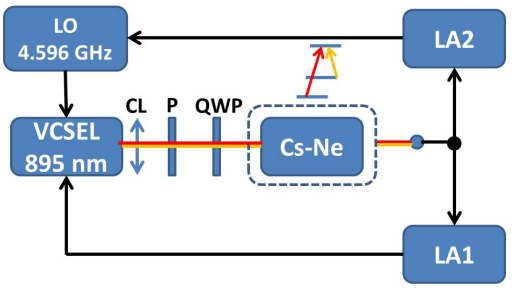

Fig. 13. Cs CPT clock experimental setup. CL: collimation lens; P: polarizer; QWP: quarter-wave plate. LA1 and LA2 are lock-in amplifiers.

1.7×10^{-7} V/$\sqrt{\text{Hz}}$. With $\nu_C = 4.596$ GHz the expected short-term stability of the clock is then $\sigma_y(\tau) = \tau^{-1/2} N/(\sqrt{2}\nu_C D) = 2.9 \times 10^{-11}\tau^{-1/2}$ at averaging times $\tau \approx 1$ s (at 80°C cell temperature). These results prove that the VCSELs are ideal candidates for the development of high-performance miniature atomic frequency standards based on CPT.

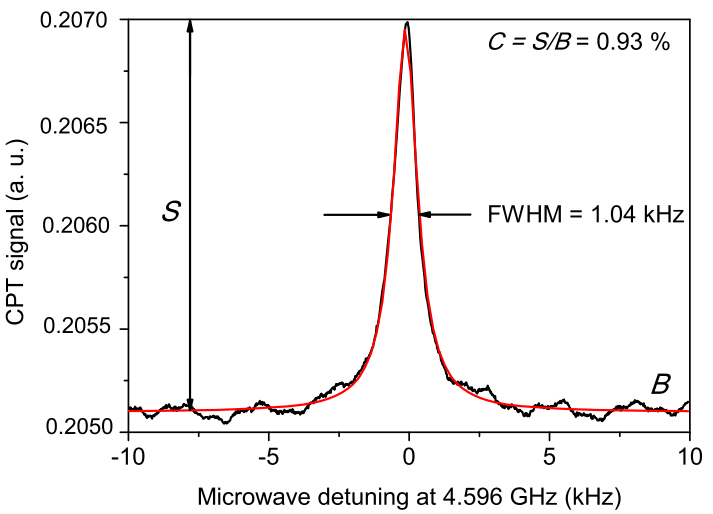

Fig. 14. CPT resonance line in the Cs–Ne microfabricated cell heated to 80°C. Experimental data are fitted by a Lorentzian profile. The resonance linewidth is 1.04 kHz and the contrast C is 0.93 %.

5. Conclusions

We have studied the spectral properties of custom-designed VCSELs emitting at 894.6 nm, in view of their suitability for the development of miniature atomic clocks based on CPT. VCSELs of two different designs were studied here: grating relief VCSELs featuring improved stability of the emitted light polarization and standard VCSELs without this grating option. Very similar optical linewidths were measured for VCSELs of both design options, in agreement with the measured frequency noise and laser frequency stabilities. Due to the similar linewidths, the frequency noise and frequency stability are concluded to be on comparable levels as well for both VCSEL designs. Analysis of the observed CPT signals shows that the grating relief VCSELs are very well suited for the development of high-performance miniature atomic clocks

based on CPT, in particular because they avoid polarization switches that can be detrimental to the performance of a CPT clock [25]. When combined with previously reported results for standard VCSELs [24], we conclude that both laser designs studied are highly suitable for use in miniature atomic clocks based on CPT on the Cs D1 line.

Acknowledgments

This work was supported by the EC within FP7 (grant no. 224132, MAC-TFC project) and by the Swiss National Science Foundation (SNSF grant no. 200020-140681). C. A. also acknowledges support from the SNSF under sinergia grant no. CRSI20_122693. The authors thank Philippe Abbé (FEMTO-ST), P. Scherler, and M. Dürrenberger (both UniNe-LTF), for technical support.